ACS APPLIED MATERIALS & INTERFACES

Research Article

www.acsami.org

Effect of Cellulose Nanocrystals (CNC) Particle Morphology on Dispersion and Rheological and Mechanical Properties of Polypropylene/CNC Nanocomposites

Vahid Khoshkava and Musa R. Kamal*

Department of Chemical Engineering, McGill University, 3610 University Street, Montreal, Quebec H3A 2B2, Canada

Supporting Information

ABSTRACT: Polypropylene (PP) nanocomposites containing spray-dried cellulose nanocrystals (CNC), freeze-dried CNC, and spray-freeze-dried CNC (CNCSFD) were prepared via melt mixing in an internal batch mixer. Polarized light, scanning electron, and atomic force microscopy showed significantly better dispersion of CNCSFD in PP/CNC nanocomposites compared with the spray-dried and freeze-dried CNCs. Rheological measurements, including linear and nonlinear viscoelastic tests, were performed on PP/CNC samples. The microscopy results were supported by small-amplitude oscillatory shear tests, which showed substantial rises in the magnitudes of key rheological parameters of PP samples containing CNCSFD. Steady-shear results revealed a strong shear thinning behavior of PP samples containing CNCSFD. Moreover, PP melts containing CNCSFD exhibited a yield stress. The magnitude of the yield stress and the degree of shear thinning behavior increased with CNCSFD concentration. It was found that CNCSFD agglomerates with a weblike structure were more effective in modifying the rheological properties. This effect was attributed to better dispersion of the agglomerates with the weblike structure. Dynamic mechanical analysis showed considerable improvement in the modulus of samples containing CNCSFD agglomerates. The percolation mechanical model with modified volume percolation threshold and filler network strength values and the Halpin−Kardos model were used to fit the experimental results.

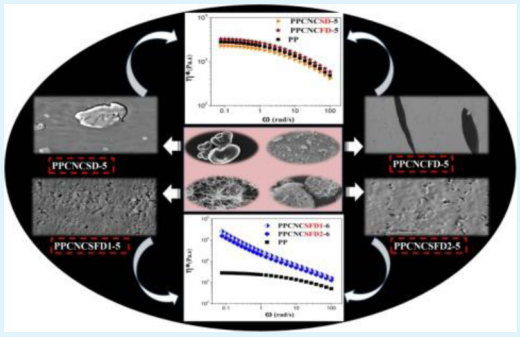

KEYWORDS: *cellulose nanocrystals (CNCs), melt dispersion, polymer nanocomposites, percolation*

INTRODUCTION

There has been growing interest in using cellulose nanocrystals (CNC) as a reinforcement in polymer systems because they are obtained from abundant and renewable resources and have interesting mechanical properties.[1,2] The preparation of polymer nanocomposites incorporating CNC has been mainly carried out using solution mixing. The negatively charged surface of CNC as a result of processing with sulfuric acid makes it possible to obtain stable CNC colloidal suspensions in water.[3,4] Therefore, water-soluble polymer matrices or water-based emulsions have been used to prepare polymer nanocomposites. This approach was used with polymers including poly(vinyl alcohol) (PVOH),[5,6] poly(furfuryl alcohol),[7] poly(styrene-*co*-butyl acrylate),[1,2,8,9] starch,[10] poly(oxyethylene) (PEO),[11] and natural rubber.[12−14] CNC particles have also been successfully incorporated into water-insoluble polymers, mainly using the solution method. Typical polymers include polypropylene (PP),[15−17] poly(vinyl chloride),[18] poly(vinyl acetate),[19] polycaprolactone,[20] poly(lactic acid) (PLA),[21−25] and epoxy resins.[26,27] Ljungberg et al.[16] examined nanocomposites based on atactic PP with three kinds of CNC via the solution method. The quality of the dispersion in PP of unmodified CNC, CNC grafted with maleated PP, and CNC modified with a surfactant was evaluated. The best dispersion was obtained using CNC coated with surfactant.

Only a few attempts have been made to prepare CNC-containing polymer nanocomposites using melt mixing, which is the industrially and environmentally favorable approach. Jiang et al.[28] prepared poly(3-hydroxybutyrate-*co*-3-hydroxyvalerate) (PHBV)/CNC nanocomposites via solution and melt mixing. It was found that solution casting produced better dispersion of CNC in the matrix compared with melt processing. Oksman et al.[21] investigated PLA/CNC nanocomposites that were produced by pumping a suspension of CNC in *N*,*N*-dimethylacetamide (DMAc)/LiCl into an extruder during melt extrusion of PLA followed by vacuum removal of the solvent. Poly(ethylene glycol) (PEG) was used as a processing aid, and PLA-*graft*-[maleic anhydride (MA)] was used as a compatibilizer. The mechanical properties of the nanocomposites did not show improvement compared with unmodified PLA because the combination of additives (DMAc/LiCl, PEG, and PLA) had a detrimental effect on the PLA. Bondeson and Oksman[29] studied nanocomposites based on

Received: January 27, 2014
Accepted: May 8, 2014
Published: May 8, 2014

   dx.doi.org/10.1021/am500577e | *ACS Appl. Mater. Interfaces* 2014, 6, 8146−8157

PLA and 5 wt % CNC as a nanofiller via melt processing. An anionic surfactant was used to improve the dispersion of CNC in the system. In another study,[22] the same authors prepared biodegradable PLA reinforced with CNC, compatibilized with PVOH, via extrusion compounding. Two feeding methods were used: (*i*) dry mixing of the PLA and CNC and (*ii*) pumping a suspension of CNC into the melt. PVOH formed a dispersed phase in the PLA. CNC nanoparticles were localized mainly in the PVOH. As a result, the thermal and mechanical properties of the PLA matrix phase did not improve upon addition of CNC. Low-density polyethylene (LDPE) and CNC grafted with various organic acid chloride compounds were melt-mixed in a twin-screw extruder.[17] It was shown that the dispersion quality improved as the length of the grafted alkyl chain increased. However, the mechanical properties did not improve substantially.

To the best of our knowledge, most attempts to prepare polymer/CNC nanocomposites and to enhance mechanical properties of the polymer via melt mixing were not successful.[21,22,28,29] This is due to the fact that CNC nanoparticles have a strong tendency to aggregate. Therefore, most successful polymer/CNC nanocomposite preparations have been limited to solution mixing. In this study, three different CNC microstructures obtained using different drying techniques were incorporated into PP via melt mixing. The morphology of the prepared PP/CNC nanocomposites was studied both directly (by microscopy) and indirectly (by rheology). The linear and nonlinear viscoelastic behavior of the PP/CNC nanocomposite samples was also studied. Furthermore, the rheological data were used to evaluate the effect of the CNC agglomerate microstructure on the dispersion level of CNC in the PP melt.

EXPERIMENTAL SECTION

Materials. The PP used in this study (Pro-fax SR549M) was supplied by LyondellBasell (Houston, TX, USA) and had a room temperature density of 0.9 g/cm^3 and a melt flow index of 11 g/10 min (2.16 kg load at 220 °C). Spray-dried cellulose nanocrystals (CNCSD) (hereafter "as received"),[30] were supplied by Forest Product Innovations (FPInnovations, Pointe-Claire, QC, Canada). The average length and thickness of CNC over 150 particles were determined using atomic force microscopy (AFM) and transmission electron microscopy (TEM) to be 171 ± 79.7 nm and 15.1 ± 5 nm, respectively.[31]The zeta potential of CNC was ca. −43 ± 4 V based on four measurements of electrophoretic mobility (Malvern Instruments Ltd.) of a CNC suspension at pH 6.

Drying of CNC. A CNC suspension was prepared by dispersing CNC powder in distilled water using a shear mixer (ULTRA-TURRAX T 25, IKA, Staufen, Germany). The CNC suspension was sonicated for 5 min in an ice bath with a tip sonicator (Qsonica Q700), to obtain the CNC dispersion. A 2.54 cm probe was used at a frequency of 20 kHz and amplitude 2, supplying ca. 750 J/g. The CNC aqueous suspension was placed overnight in a refrigerator set at −50 °C and then freeze-dried using a Labconco 2.5 L freeze dry system to obtain freeze-dried CNC. Spray-freeze-dried CNC was produced by first spraying the CNC suspension into a container containing liquid nitrogen agitated with a magnetic stirring bar. The resultant slurry was lyophilized at −52 °C and 0.05 mbar for a period of time (24−72 h).

Preparation of Polymer/CNC Nanocomposites. Melt compounding was performed in an internal batch mixer (Rheocord 9000, Haake) with a total capacity of 60 mL. Melt mixing was carried out at 190 °C and a rotor speed of 60 rpm for 10 min under a nitrogen atmosphere. As received, freeze-dried, and spray-freeze-dried CNC were fed separately in different experiments into the internal batch mixer after polymer granules were melted. Finally, each mixture was collected for further characterization after cooling to room temperature. Table 1 summarizes the nomenclature used to identify different samples.

Table 1. Nomenclature Used for Samples in This Article

label	drying method	wt % CNC
PPCNCSD-5	spray drying	5
PPCNCFD-5	freeze drying	5
PPCNCSFD1-*i*	spray-freeze drying from a 1 wt % CNC aqueous suspension	*i* = 1.5, 2.5, 5, 6
PPCNCSFD2-*i*	spray-freeze drying from a 2 wt % CNC aqueous suspension	*i* = 2.5, 5, 6

Characterization. *Morphological Studies.* Field-emission scanning electron microscopy (FE-SEM) using a Hitachi S-4700 scanning electron microscope operated at 2 kV was used to examine the topography of CNC powders prepared by the three different drying techniques. Prior to electron microscopy, the CNC powders were coated by gold−palladium vapor deposition for a period of 30 s.

SEM (JSM-7400F, JEOL, Tokyo, Japan) was used to evaluate the distribution of CNC in the PP matrix. The cryo-fractured surfaces of specimens were coated with gold vapor and observed by SEM.

AFM was performed on cryo-microtomed surfaces of samples that were cut with a glass knife. The AFM images were captured using a commercial scanning probe (Dimension 3100) equipped with a Nanoscope IIIa controller (Veeco Digital Instruments, Santa Barbara, CA, USA) in tapping mode under ambient conditions. Silicon tips (Veeco model RTESP) with spring constants of 20−80 N/m and resonant frequencies of 250−350 kHz were used in the tapping mode.

Rheological Measurements. Small-amplitude oscillatory shear (SAOS) and steady shear tests were performed using a stress-controlled rheometer (Physica MCR 500, Anton Paar, Graz, Austria) with parallel plate geometry (25 mm plate diameter) at 190 °C under a nitrogen atmosphere. Disk-shaped samples were positioned in the parallel plate fixture and left for 10 min to minimize any residual stress resulting from sample preparation. The gap was set at 1 mm by gradually squeezing the sample. Both neat PP and PP/CNC nanocomposites were found to be stable at 190 °C for a period of over 2 h. Hence, thermal degradation was considered to be negligible during the rheological measurements.

In SAOS experiments, the linear viscoelastic region was first determined using a strain sweep from 1 to 100% at a constant frequency of 1 rad/s. The linear viscoelastic region was identified as the region in which the elastic modulus of the sample experienced less than 5% reduction. Then SAOS tests were conducted in the frequency range of 0.05−100 rad/s at 190 °C. The results provided by this test included complex viscosity (η^*), elastic modulus (G'), and loss modulus (G''). These parameters provide a detailed description of the viscoelastic behavior of the sample.

For further microstructural study, stress relaxation and preshearing tests were performed on PP/CNC nanocomposites. For stress relaxation tests, specimens were subjected to a small strain of 0.5% and the stress was recorded versus time. The effect of preshearing on the microstructure of the PP/CNC nanocomposites was studied by subjecting each sample to a constant shear rate (0.1 or 1 s^{-1}) for 200 s. SAOS measurements were then carried out without any rest time between the preshearing step and the frequency sweep test.

Steady shear tests in the 5×10^{-3} to 1 s^{-1} range were carried out to investigate the nonlinear behavior of the polymeric nanocomposite samples.

Mechanical Properties. Dynamic mechanical thermal analysis (DMTA) tests were performed on compression-molded samples with thickness, width, and height of 2 mm, 20 mm, and 65 mm, respectively, using a DMA 2980 analyzer (TA Instruments, New Castle, DE, USA). The specimens were tested in the dual cantilever bending mode at an amplitude of 30 μm, a frequency of 1 Hz, and a heating rate of 3 °C/min over the range from −80 to 160 °C under a nitrogen atmosphere.

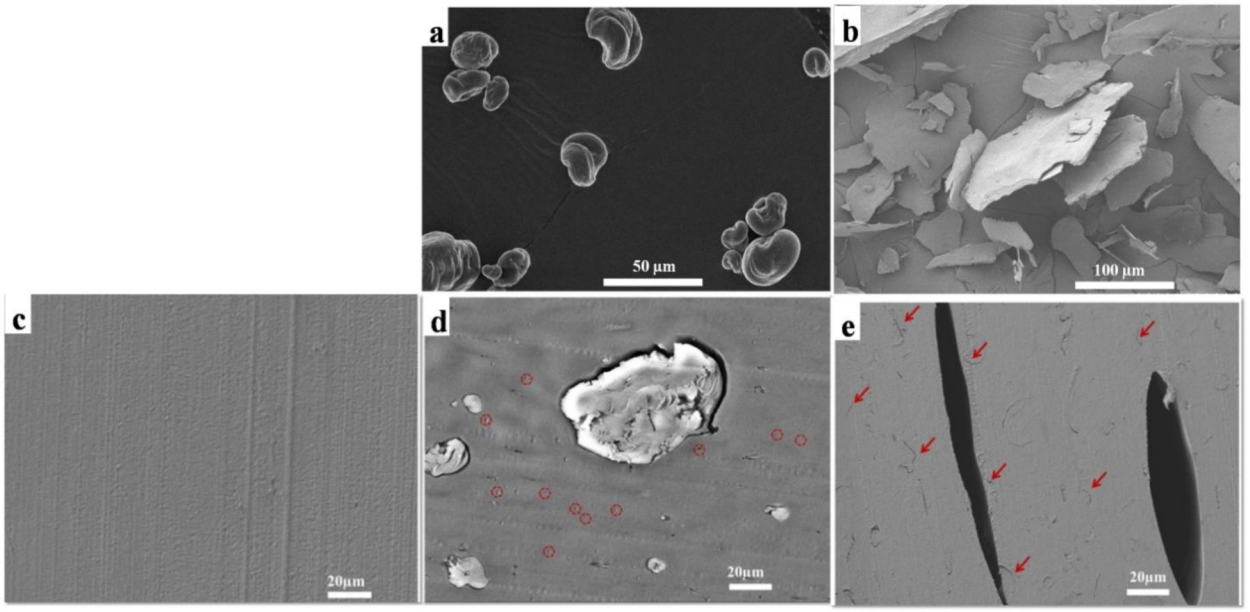

Figure 1. SEM images of (a) spray-dried CNC (CNCSD), (b) freeze-dried CNC (CNCFD), (c) neat PP, (d) PP containing 5 wt % CNCSD (PPCNCSD-5), and (e) PP containing 5 wt % CNCFD (PPCNCFD-5).

RESULTS AND DISCUSSION

Morphological Studies by Microscopy. Morphological characterization results are shown in Figures 1 to 3. Figure 1 shows SEM results for (a) spray-dried CNC (CNCSD), (b) freeze-dried CNC (CNCFD), (c) neat PP, (d) PP containing 5 wt % CNCSD (PPCNCSD-5), and (e) PP containing 5 wt % CNCFD (PPCNCFD-5). In spray drying, CNC agglomeration is caused by capillary, hydrogen-bonding, and van der Waals forces. On the other hand, ice crystal growth plays a key role in CNC agglomeration during freeze drying. The presence of CNC agglomerates in Figure 1d (spherical-shaped CNCSD) and Figure 1e (lamella/sheetlike CNCFD) indicates subtle particle size reduction and poor deagglomeration and dispersion of the CNC particles generated using conventional drying methods (spray and freeze drying) of CNC suspensions. It seems that almost insignificant polymer melt infiltration took place within the compact and dense structures of spray- and freeze-dried CNC agglomerates. The SEM results also reveal that some small fragments of CNC agglomerates were detached from large agglomerates, as shown by circles and arrows in Figure 1d,e. SEM images of spray-freeze-dried CNC prepared from 1 wt % (CNCSFD1) and 2 wt % (CNCSFD2) CNC suspensions are shown in Figure 2a,b, respectively. Unlike spray and freeze drying, less agglomeration occurs in the spray-freeze drying technique, and the dispersed state of CNC in water can be frozen in. Thus, spray-freeze drying of the CNC suspension resulted in a powder with porous or network structures. The key parameter controlling these structures is the CNC concentration prior to spray-freeze drying. Different from the cases in Figure 1, these more open and porous particle morphologies result in high efficiency of deagglomeration and dispersion of CNCSFD in the PP matrix for both CNCSFD1 (Figure 2c,e) and CNCSFD2 (Figure 2d,f). Dissimilar to CNCSD and CNCFD, the low agglomerate strength of the porous, open structures and the high potential for polymer melt infiltration into these structures are the main reasons for substantially improved dispersion with CNCSFD. The small holes in Figure 2c–e are possibly CNCSFD nanoparticles that

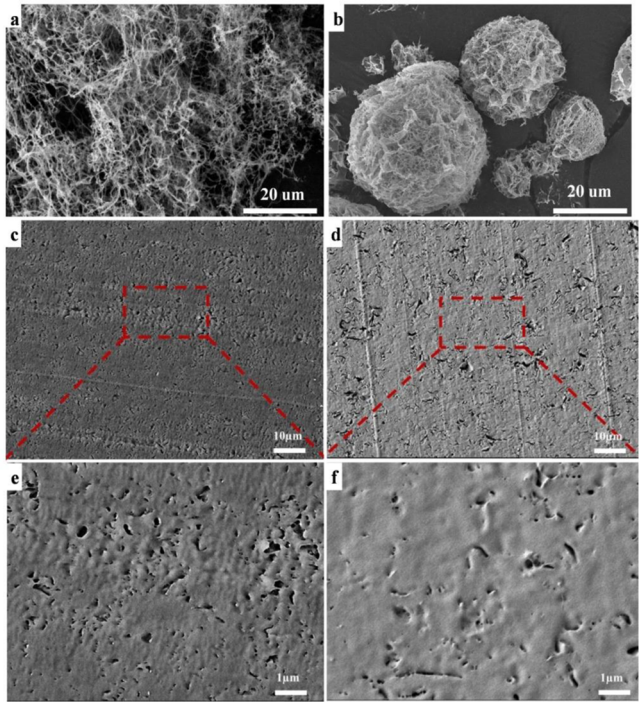

Figure 2. SEM images of (a) CNCSFD1 and (b) CNCSFD2 and of (c, e) PPCNCSFD1-5 and (d, f) PPCNCSFD2-5 at (c, d) low and (e, f) high magnification.

were pulled out during microtoming. Figure 2 also compares the dispersion states of CNCSFD1 and CNCSFD2 agglomerates in PP. The CNCSFD1 number density in PP (Figure 2c,e) is higher than that of CNCSFD2 (Figure 2d,f). This is due to structural differences between the CNCSFD1 and CNCSFD2 agglomerates. The former agglomerates have a more open structure and thus are more susceptible to polymer infiltration and dispersion.

Figure 3 displays AFM images of PPCNCSFD1-5. The AFM phase image (Figure 3b) shows better contrast for CNC

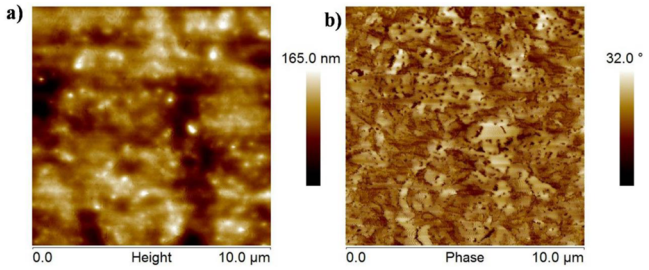

Figure 3. AFM (a) height and (b) phase images of PPCNCFD1-5.

compared with the height image (Figure 3a). Features seen in Figure 3b include CNC particles detached from the PP surface during microtoming as well as those that remained attached to the PP surface. The latter, particularly those with thicknesses smaller than ca. 500 nm, cannot be seen in the SEM images because of the nonconductive nature of both PP and CNC in addition to the presence of a thin layer of gold coating (ca. 20–30 nm) due to SEM sample preparation. This explains the higher CNC particle number density observed in the AFM images compared with the SEM image (Figure 2f).

Rheological Measurements. *SAOS Results. Complex Viscosity.* Strain amplitude sweep tests were used to determine the linear viscoelastic region (see the Supporting Information). The results of measurements of complex viscosity (η^*) versus angular frequency (ω) are shown in Figure 4. Addition of 5 wt % CNCSD or CNCFD to the PP melt did not change the complex viscosity, which was almost superimposed with the PP curve (Figure 4a). Henceforth, in the rest of this article, only results obtained for PP containing CNCSFD are compared and discussed. The complex viscosity increased monotonically upon incorporation of CNCSFD1 agglomerates in the PP melt (Figure 4b). Moreover, there is a noticeable upward shift in complex viscosity at all frequencies at 5 and 6 wt % loadings of CNCSFD1 in comparison with lower concentrations.

The samples displayed an apparent yield stress at low angular frequency for concentrations of 2.5 wt % and above. The incidence of yield stress is more obvious when complex viscosity is plotted versus complex modulus (Figure 5). Similar behavior has been reported for polymers that are highly filled (more than 30 wt %) with microfillers.[32−34] Thus, the source of yield stress in PP/CNCSFD1, especially at such low concentrations (above ca. 2.5 wt %) could be attributed to the interconnection of anisotropic nanoparticles within the PP matrix. The apparent yield stress (σ_y) can be determined by applying the modified four-parameter Cross model to the experimental data:

$$\eta = \frac{\sigma_y}{\omega} + b(1 + c\omega^d)^{-1} \quad (1)$$

where b (Pa·s), c (s), and d (dimensionless) are model parameters. The results of curve fitting based on eq 1 are plotted as black solid lines in Figure 4b, and the obtained model parameters are listed in Table 2. It is noteworthy that PP samples containing CNCSFD2 showed lower yield stress values than samples containing CNCSFD1. This suggests that CNCSFD1 agglomerates formed a stronger network within the PP matrix as a result of the better dispersion level, as discussed earlier.

It is also possible to make a rough estimate of the CNC diameter on the basis of the yield stress values estimated from rheological measurements. The formation of a network at CNC

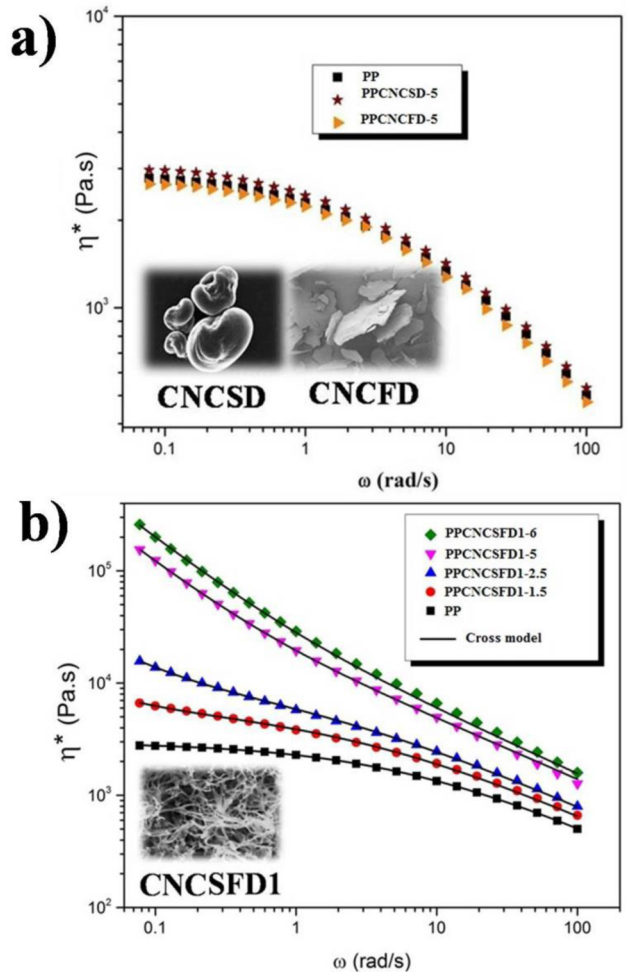

Figure 4. Plots of complex viscosity vs angular frequency for (a) PP, PPCNCSD-5, and PPCNCFD-5 and (b) PP and PP containing CNCSFD1 agglomerates. The insets show SEM images of spray-dried (CNCSD), freeze-dried (CNCFD), and spray-freeze-dried (CNCSFD) CNC agglomerates.

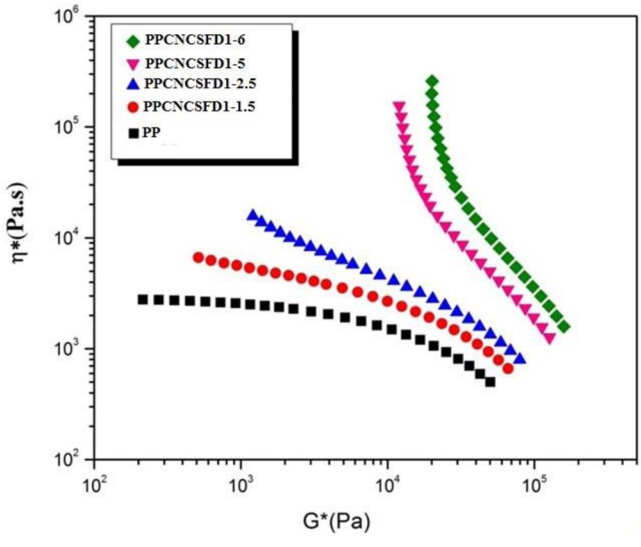

Figure 5. Plot of complex viscosity vs complex modulus for PP and PP containing CNCSFD1.

dx.doi.org/10.1021/am500577e | ACS Appl. Mater. Interfaces 2014, 6, 8146−8157

Table 2. Values of the Paramenters in the Cross Model (eq 1) Used for Curve Fitting of the Experimental Complex Viscosity

material	σ_y (Pa)	b (Pa·s)	c (s)	d
PP	0.00	2980.96	0.31	0.60
PPCNCSFD1-1.5	117.02	5837.30	0.55	0.58
PPCNCSFD1-2.5	602.28	9568.82	0.82	0.57
PPCNCSFD1-5	10999.14	16802.50	0.96	0.55
PPCNCSFD1-6	18544.49	20498.69	1.1	0.55
PPCNCSFD2-2.5	144.41	7760.99	0.69	0.55
PPCNCSFD2-6	7763.22	6939.30	0.41	0.56

concentrations above the percolation threshold may be considered to be due to the agglomeration of interconnecting of CNC clusters to form an infinite cluster spanning the whole polymer matrix.[35] This network can be further assumed to be composed of randomly distributed spheres with radius R encapsulating N CNC particles with particle volume V_p.[36] The percolation threshold of randomly packed overlapping spheres occurs at a volume fraction (ϕ_{RPS}) of 0.32.[37] Thus, the CNC volume fraction enclosed in each sphere (ϕ) is calculated as

$$\frac{NV_p}{\frac{4}{3}\pi R^3} = \frac{\phi}{\phi_{RPS}} \tag{2}$$

The particle agglomerate strength can be estimated using Rumpf's equation:

$$\sigma = \frac{1-\epsilon}{\epsilon}\frac{2A_H}{3\pi z_0^2 D^2} \tag{3}$$

in which

$$A_H = 2\pi z_0^2 \gamma_i \tag{4}$$

where ϵ, A_H, Z_0, D, and γ_i are the porosity, Hamaker constant, "cutoff" distance, particle diameter, and surface energy, respectively. The CNC surface energy was estimated to be 18.6 mJ/m^2.[31] For simplicity, CNC particles with the cross orientation were considered to derive eq 3. The porosity of spherical units of the three-dimensional (3D) network could also be estimated as

$$1-\epsilon = \frac{NV_p}{\frac{4}{3}\pi R^3} \tag{5}$$

Finally, the yield stress can be related to the strength of spherical particles containing CNC particles by assuming that the system will experience yield if the applied hydrodynamic stress is higher than the strength of these spheres. A CNC particle radius of ca. 102 nm was obtained from the inverse of the slope of a plot of σ_y versus $2(1-\epsilon)A_H/(3\pi z_0^2\epsilon)$ (see Figure S.2 in the Supporting Information). This value is an approximation of the effective CNC agglomerate diameter leading to the above rheological behavior.

Storage and Loss Moduli. The results of SAOS tests for storage and loss moduli are presented in Figure 6. The classical viscoelastic behavior of a homogeneous polymer solution/melt is distinguished by $G'' > G'$, where at low frequency (in the terminal region), $G' \propto \omega^2$ and $G'' \propto \omega$.[38] The PP sample showed liquidlike behavior at low frequency ($G'' > G'$), where the slopes of G' and G'' were 1.60 and 0.94, respectively. Deviation from the exponents of 2 and 1 for the storage and loss moduli, respectively, could be attributed to the

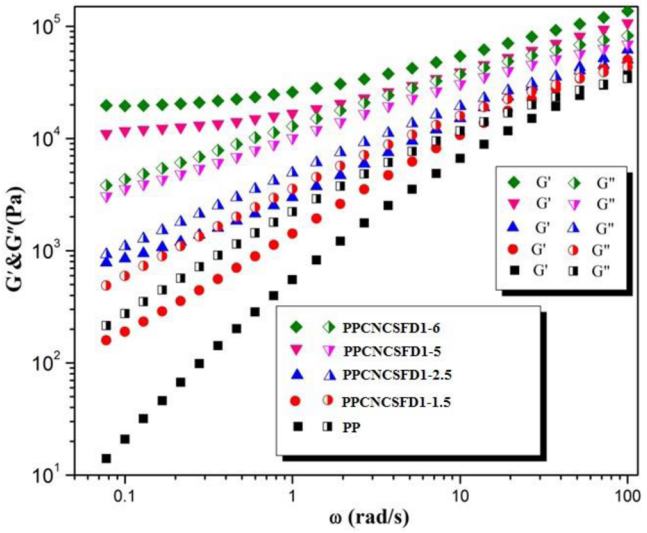

Figure 6. Storage and loss moduli as functions of angular frequency for PP and PP containing CNCSFD1.

polydispersity of the commercial PP resin. It should be emphasized again that there was no difference between the rheological properties of PP, PPCNCFD-5, and PPCNCSD-5. Figure 6 also shows that at low frequency both the storage and loss moduli increased upon incorporation of CNCSFD1 in PP. For instance, adding just 2.5 wt % CNCSFD1 led to a 1 order of magnitude increase in the storage modulus at low frequency, which is an indication of percolation in rheological properties. The storage modulus was more sensitive to the presence of CNCSFD1 than the loss modulus. A similar trend has been reported for other polymer nanocomposite systems.[39,40] Furthermore, the slopes of both the loss modulus and the storage modulus versus angular frequency in the terminal region were lowered by addition of CNCSFD1 to PP. For instance, the slope of the storage modulus versus frequency decreased from 0.94 for PP to 0.03 for PPCNCSFD1-6. The weak dependence of the storage modulus on the angular frequency (i.e., the gentle slope) observed for CNCSFD1 at concentrations above 2.5 wt % is a characteristic of solidlike behavior.[39−43]

Figure 6 shows that for PPCNCSFD1-2.5, G' would cross G'' upon extrapolation of the data to frequencies lower than 0.1 rad/s. The intersection approximately represents the percolation threshold at which nanoparticles start interacting.[40,42−44] On the other hand, for PPCNCSFD1-5 and PPCNCSFD1-6, the storage modulus was higher than the loss modulus over most of the frequency range. The low-frequency (0.07 rad/s) storage and loss moduli scaled with the volume fraction as $G' \sim \phi_v^{3.5}$ and $G'' \sim \phi_v^{3.5}$, respectively. The scaling exponents reported for other polymer nanocomposite systems are in the range of 2.4 to 4.7 for storage modulus and 2.2 to 3.9 for loss modulus.[45] It is interesting that storage modulus was higher than loss modulus at all tested frequencies. This is an indication of dominance of solidlike relaxation behavior. Shih et al.[35] characterized the fractal structure of colloidal gels as a connection of closely packed fractal flocs through the matrix. Employing the scaling theory developed for polymer solutions, they showed that

$$G' \sim \phi^{(3+x)/(3-d_f)} \tag{6}$$

and

$$\gamma_c \sim \phi^{-(1+x)/(3-d_f)} \quad (7)$$

where d_f and x are the fractal dimension and the power by which the number of particles per floc scales with the floc size. Using data points above the percolation threshold and applying simple regression analysis affords values of 1.7 and 1 for d_f and x, respectively. The value of 1.7 for the fractal dimension indicates that the 3D network consists of porous and open flocs.

Damping Factor (tan δ). Figure 7 shows a plot of the damping factor tan δ (where δ is the phase angle) versus frequency for pure PP and PP filled with CNCSFD1. The transition from liquidlike to solidlike behavior occurs at the crossover frequency (ω_c), at which tan δ = 1. The inverse of this crossover frequency is equivalent to the characteristic relaxation time of the polymer chain (λ_c).[38] For the PP matrix, ω_c and λ_c were 72 rad/s and 0.08 s, respectively. The crossover frequency decreased to 52 rad/s for PPCNCSFD1-1.5. This implies that polymer chain relaxation was retarded by the presence of CNCSFD1. For the PPCNCSFD1-2.5 sample, two crossover frequencies were observed at 39 and 0.01 rad/s, where the second crossover frequency was obtained after extrapolation. Therefore, one could draw the conclusion that percolation occurred at a CNCSFD1 concentration of ca. 2.5 wt %.

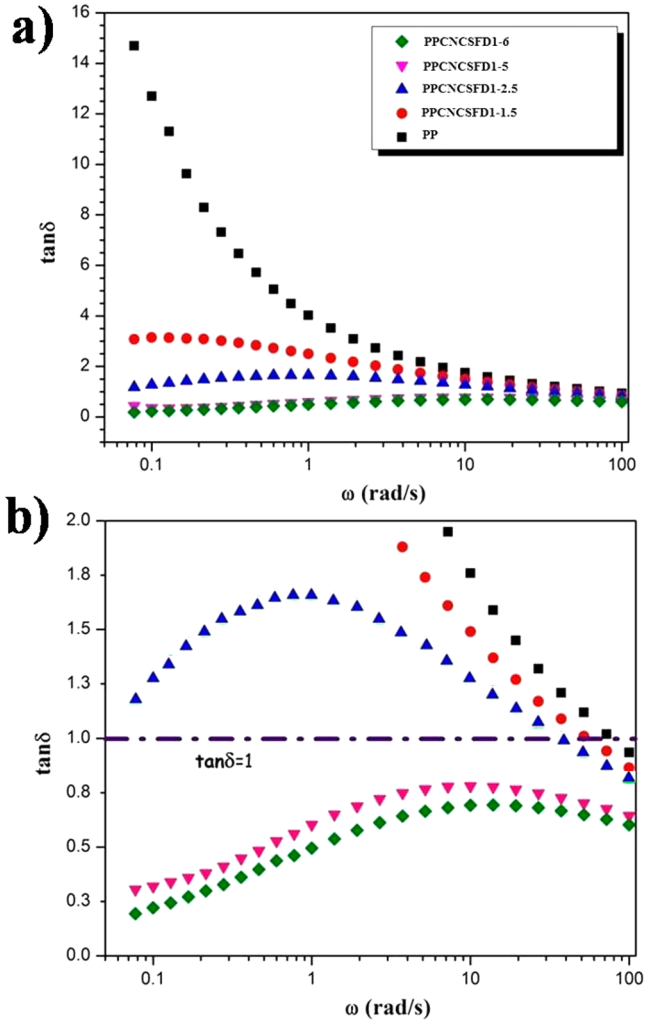

Figure 7. (a) Plot of tan δ vs angular frequency for PP and PP containing CNCSFD1. (b) Closer view of the plot in (a).

Different behavior was observed for PPCNCSFD1-5 and PPCNCSFD1-6. The damping factor was almost independent of frequency, and the value of tan δ was always less than 1. Indeed, this is a typical behavior of elastic materials.

CNC Concentration and Network Structure. For filled polymer matrices, particularly those filled with anisotropic nanoparticles, there are two kinds of responses to applied force. At low concentration (the dilute regime), the polymer matrix controls the rheological properties. Polymer relaxation is affected by the presence of nanoparticles, as discussed earlier (Figure 7). The other responses are related to micro/mesostructure or network development at higher concentration due to colloidal van der Waals nanoparticle−nanoparticle and/or polymer−filler interactions.[40−43] At low CNCSFD1 concentration (below 2.5 wt %), the main mechanism for increasing the low-frequency rheological properties, such as the complex viscosity (Figure 4b) and the storage and loss moduli (Figure 6), could be attributed to the effect of the nanoparticles on the polymer chain mobility. In fact, the interfacial area created by the nanoparticles would influence the relaxation of the polymer chains, particularly those that are adjacent to the PP−CNCSFD1 interface/interphase. This results in an increase in polymer chain relaxation time, as seen in the tan δ results for PPCNCSFD1-1.5 and PPCNCSFD1-2.5 in Figure 7. As mentioned earlier, adding 5 wt % spray-dried or freeze-dried CNC did not have much effect on the low-ω rheological properties of PP. However, these properties were increased by the addition of just 1.5 wt % CNCSFD1. As mentioned earlier (Figure 2), the porous weblike microstructure of CNCSFD1 exhibited good dispersion in PP.

PPCNCSFD1-5 and PPCNCSFD1-6 exhibited significantly different rheological behavior compared with the systems at lower CNCSFD concentrations. At these higher concentrations, nanoparticle−nanoparticle distances could be in the range of van der Waals interactions (less than ca. 100 nm) or comparable with the polymer chain radius (ca. 10−30 nm), and the nanoparticles could form a 3D network, as already reported for many polymer nanocomposite systems.[35,39−43] The connectivity or percolation of CNC particles could be inferred from the morphological observation illustrated in Figure 3b as a result of the high particle number density. As a result, particle−particle interactions dominate the low-frequency viscoelastic response. The polymer chains could also play a role in the particle interconnectivity. They may bridge particles where the interparticle distance is small but not small enough for particles to overlap. Therefore, at high concentrations of CNCSFD1, the formation of a network structure caused by particle−particle interactions and/or particle−polymer interactions is responsible for the low-frequency rheological properties. The presence of this network determines the following aspects of the rheological behavior of the system:

- short linear viscoelastic region (Figure S.1 in the Supporting Information)
- high resistance to flow reflected by an upturn in viscosity at low frequency (Figure 4b)
- G' higher than G'' over the whole range of tested frequencies (Figure 6)
- tan δ less than 1 over the whole range of tested frequencies (Figure 7)

Preshearing. The effect of preshearing or flow history on the viscoelastic properties of PP and PPCNCSFD1-6 samples was investigated. Samples were sheared at 0.1 or 1 s^{-1} for 200 s. Figure S.3a in the Supporting Information displays complex viscosity as a function of frequency without and with preshearing for PP. The effect of preshearing was almost negligible for PP, and the curves were almost identical. On the other hand, the complex viscosity was lowered after preshearing for PPCNCSD1-6 (Figure S.3b in the Supporting Information). Greater reductions in the complex viscosity and storage modulus were observed as the shear rate increased from 0.1 to 1 s^{-1}. This could be related to the destruction of the percolated network after the application of high strains (20 and 200), which are beyond the critical strain shown in Figure S.1 in the Supporting Information. The extent of network damage depends on the total strain imposed on samples during preshearing. Structure or network damage due to flow-induced orientation is the main reason for the reduction. These results suggest the formation of a structure or network that determines the linear viscoelastic behavior at low frequencies at higher CNCSFD1 concentrations. Similar results have been reported for polymer nanocomposites of anisotropic nanoparticles above the percolation threshold.[42−46]

Stress Relaxation. Stress relaxation was used as a probe to evaluate the long-time behavior of the systems. In this test, a step shear strain of 0.5% was applied, and the response of the material was recorded with time. Figure S.4 in the Supporting Information shows the results of the stress relaxation experiment for both the pure matrix and PPCNCSFD1-6 after a step shear strain of 0.5%. PP and PPCNCSFD1-6 showed similar values of the relaxation modulus at very short times, corresponding to the value obtained at high angular frequency in the SAOS test. Moreover, the pure matrix relaxed very rapidly in less than 2 s, while PPCNCSFD1-6 relaxed slowly, requiring more than 3000 s. The slope of the stress relaxation modulus was constant after 10 s of the experiment, signifying that there is a plateau in the modulus. This plateau is more obvious when the result is plotted on a semilog scale (Figure S.4b in the Supporting Information).

Effect of CNCSFD Structure on the SAOS Results. As shown in Figure 2a,b, depending on the CNC aqueous concentration, two different types of microstructure/morphology were obtained from the spray-freeze drying technique. At low concentrations (CNCSFD1), a weblike microstructure was formed, while a spherical foam structure was obtained at higher concentrations (CNCSFD2). The effect of the CNCSFD particle microstructure on the linear melt viscoelastic properties was studied.

Linear viscoelastic tests were used to study the effect of the CNC agglomerate microstructure on the PP melt viscoelastic properties. Figure 8 compares the results regarding complex viscosity and storage modulus for PP containing CNCSFD1 and CNCSFD2 at two different concentrations (2.5 and 6 wt %). Both the complex viscosity and storage modulus were superior for the PP/CNCSFD1 system. However, the complex viscosity and storage modulus values for PP/CNCSFD2 were significantly higher than for spray-dried and freeze-dried CNC (Figure 4a). This indicates that regardless of the CNCSFD structure, the impact of CNCSFD particles on the rheological properties of PP is higher than that of freeze-dried and spray-dried CNC. Considering the results for a concentration of 2.5 wt %, the total surface area created by CNCSFD1 should be higher than that created by CNCSFD2. Consequently, the

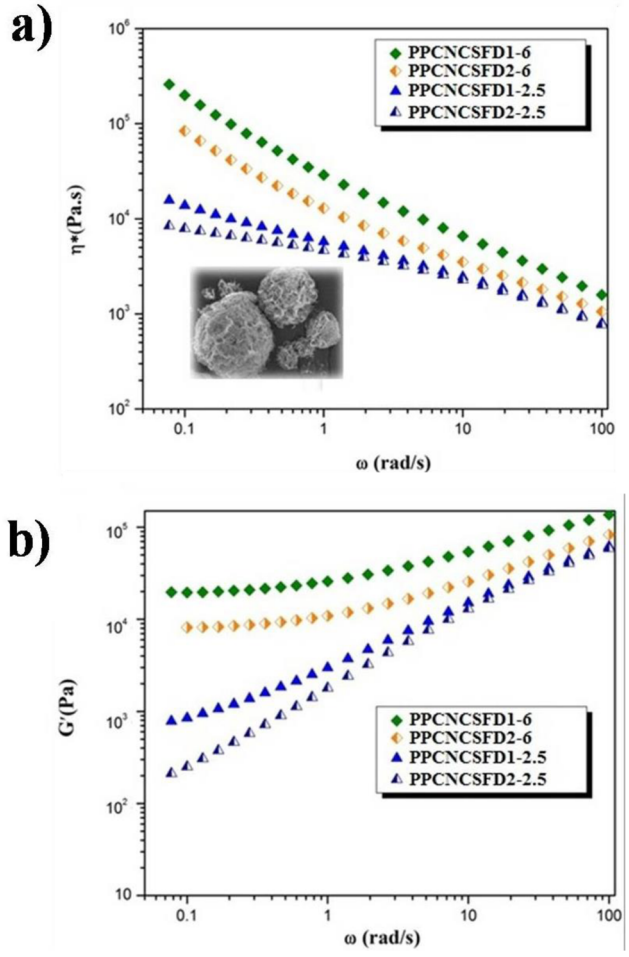

Figure 8. Effect of CNCSFD agglomerate structure on (a) the complex viscosity and (b) the storage modulus of PP. The inset in (a) shows an SEM image of the CNCSFD2 agglomerate.

dispersion level in PP/CNCSFD1 should be better than that in PP/CNCSFD2. At concentrations above percolation, the rheological properties are controlled by the network made of nanoparticles. Therefore, the strength of the network is controlled by nanoparticle−nanoparticle and polymer−nanoparticle interactions. The above results indicate that CNCSFD1 is more effective than CNCSFD2 in raising the magnitudes of the above rheological properties. Moreover, it could be concluded that the dispersion level of CNCSFD1 is higher than that of CNCSFD2, which is in agreement with the SEM results (Figure 2). The differences in rheological responses could be related to the difference in porosity of the structure as well as the cohesive strength of the agglomerates prior to melt mixing. CNCSFD1 had a weblike structure with interconnected nanoscale fibers (Figure 2a). This facilitated polymer infiltration, and less deagglomeration effort was required. On the other hand, in CNCSFD2, micrometer-sized spherical agglomerates with foamlike structure were formed (Figure 2b). As a result, more energy was required to produce the degree of breakup needed to achieve good dispersion.

Steady-State Shear. The nonlinear rheological properties of PP containing CNC were also studied. The results for steady-shear viscosity as a function of shear rate are exhibited in Figure 9. PP, PPCNCSD-5, and PPCNCFD-5 showed typical Newtonian behavior at low shear rates (Figure 9a). As in the SAOS tests, there was no substantial difference in the steady-

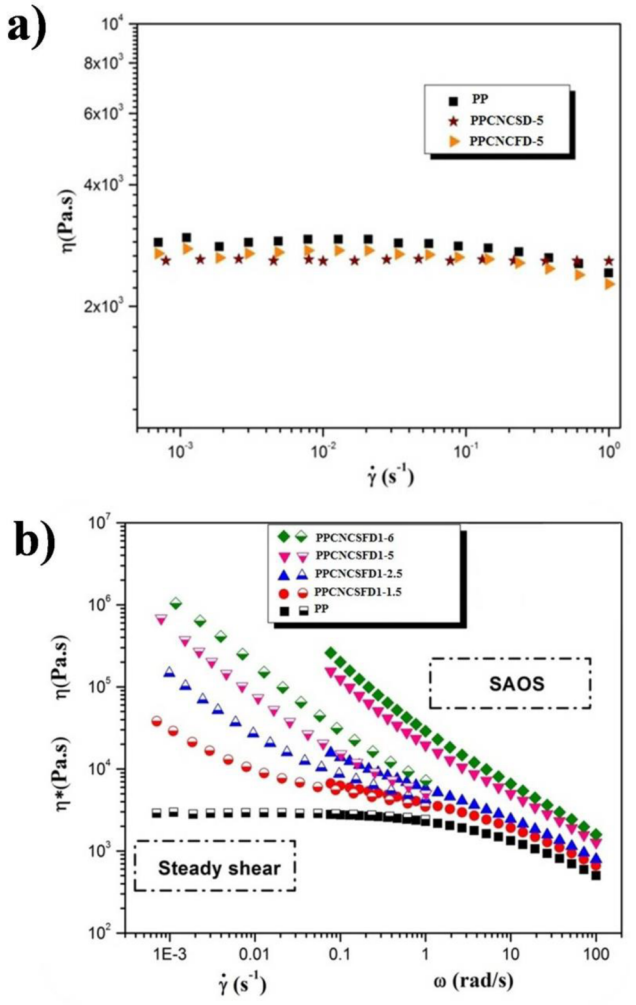

Figure 9. (a) Steady-shear viscosity vs shear rate for PP, PPCNCSD-5, PPCNCFD-5. (b) Steady-shear and complex viscosities of PP and PP containing CNCSFD1.

shear rheological behavior of PP and samples containing spray-dried or freeze-dried CNC. However, PP containing CNCSFD1 showed significant shear thinning behavior at low shear rates, where the steady-shear viscosity divergently increased with decreasing shear rate (Figure 9b). At high shear rates, the viscosities of the nanocomposites approached the value for the PP matrix. Orientation of anisotropic particles and/or network damage induced by the flow field could be the main reason(s) for shear thinning.

The steady-shear viscosity can be estimated from the complex viscosity in SAOS tests by using the empirical Cox–Merz rule at equivalent shear rate and frequency (Figure 9b). For PP and PPCNCSD5, the results for complex modulus at low frequency and steady shear superimposed. On the other hand, the Cox–Merz rule failed for PP containing CNCSFD1. This behavior is typically observed for liquid-crystalline polymers and highly filled suspensions. Similar behavior has been reported for other polymer nanocomposite systems.[39,40,42,47]

Thermal Stability of PP/CNC Nanocomposites. Thermogravimetric analysis (TGA) and derivative thermogravimetric analysis (DTGA) tests were carried out for spray-dried CNC under a nitrogen atmosphere (Figure S.5 in the Supporting Information). Similar results were obtained for freeze-dried and spray-freeze-dried CNC. The temperatures for 5 wt % weight loss and the locations of the DTGA peak were 298 and 312 °C, respectively. The CNC water content was 3.6 wt %, and the amount of CNC ash content was negligible. CNC degradation starts at 298 °C. Figure 10a shows TGA

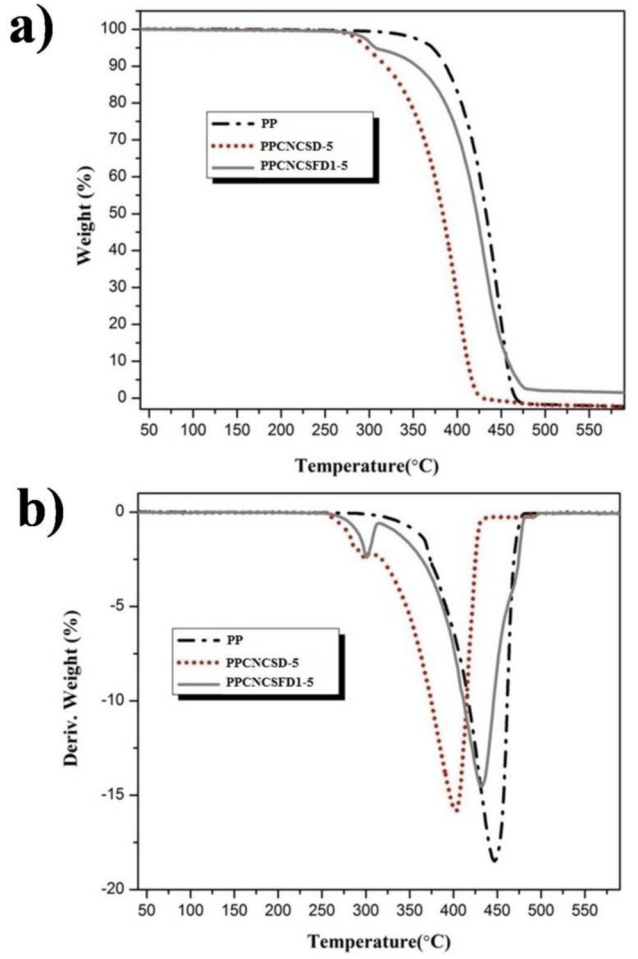

Figure 10. (a) TGA and (b) DTGA results for PP (dash-dotted), PPCNCSD-5 (dotted), and PPCNCSFD1-5 (solid).

results for pure PP, PPCNCSD-5, and PPCNCSFD1-5. The curve for PPCNCFD-5 is not shown since it overlapped with that for PPCNCSD-5. The onset temperature of degradation for PP was ca. 445 °C. On the other hand, the onset temperatures for PPCNCSD-5 and PPCNCSFD1-5 were 370 and 400 °C, respectively. Moreover, a step reduction in the weight loss graph was also observed. It appeared as a small peak in the DTGA curve in Figure 10b. The inflection temperatures for PPCNCSD-5 and PPCNCSFD1-5 were 298 and 303 °C, respectively. The main DTGA peak temperatures for PP, PPCNCSD-5, and PPCNCSFD1-5 were 447 °C, 402 °C, and 430 °C, respectively. It seems that CNCSFD1 had a less detrimental effect on the degradation behavior of PP than CNCSD. This may be attributed to the encapsulation of more CNC nanoparticles in porous CNCSFD1 with PP chains. As a result, the thermal stability of systems incorporating CNCSFD1 is likely to be higher than that of systems incorporating the spray-dried CNC agglomerates.

Dynamic Mechanical Analysis (DMA). Figure 11 displays DMA results for PP, PPCNCSD-5, PPCNCSFD1-5, and PPCNCSFD2-5. The DMA profile for the PPCNCSD-5

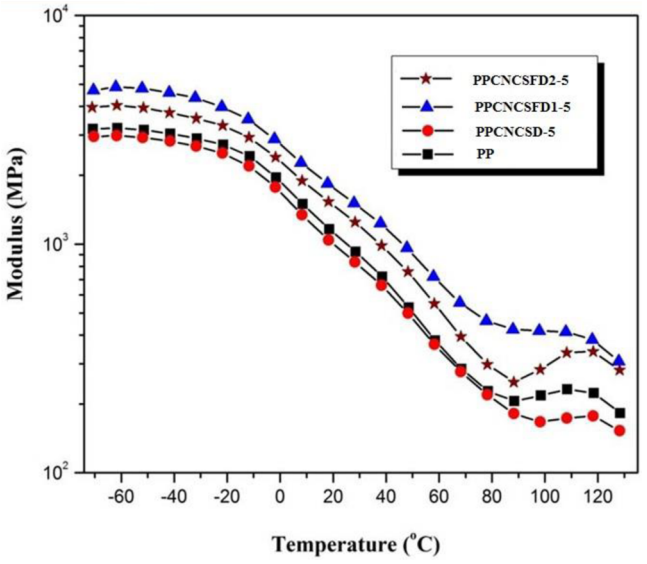

Figure 11. Storage modulus (semilog) vs temperature for PP, PPCNCSD-5, PPCNCSFD1-5, and PPCNCSFD2-5.

sample is very similar to that for the PP resin, indicating only a small impact of the CNC on the base resin (Figure 11). As in the case of the rheological behavior, incorporation of spray-dried (as received) CNC had no effect on the mechanical properties of the PP matrix. On the other hand, samples containing CNCSFD1 and CNCSFD2 exhibited significantly higher storage modulus values over the entire range of temperatures. At room temperature (25 °C), the modulus values for PPCNCSFD1-5 and PPCNCSFD2-5 were ca. 60% and 30% higher, respectively, than for the neat PP. In accordance with the rheology results, spray-freeze drying of the CNC suspension prior to compounding caused a substantial and measurable change in the dynamic mechanical behavior. PP samples containing CNCSFD1 showed higher DMA moduli than those containing CNCSFD2. This is mainly due to the difference in the microstructures of the powders. CNCSFD1 has nanofibers or filaments with very long aspect ratio. Therefore, it has the potential to modify the properties significantly. CNCSFD2 particles are very porous spherical agglomerates and more effort is required for polymer infiltration and particle breakup/deagglomeration.

The main reinforcing mechanism of the CNC is assigned to the presence of a percolated network within the polymeric systems.[1,48] The series−parallel model of Takayanagi[49] was modified in order to take account of the percolation observed in the experimental results at temperatures higher than the glass transition temperature (T_g) of the host polymer.[1] Accordingly, the shear modulus of the composite (G_c) is expressed by

$$G_c = \frac{(1 - 2\psi + \psi\phi)G_p G_{np} + (1 - \phi)\psi G_{np}^{\ 2}}{(1 - \phi)G_{np} + (\phi - \psi)G_p} \tag{8}$$

where ψ, ϕ, G_p, and G_{np} are the percolation volume fraction of the rigid phase formed by nanoparticles, the volume fraction of nanoparticles, the shear modulus of the polymer, and the shear modulus of the rigid phase, respectively.[1] G_{np} in eq 8 is the shear modulus of the network of CNC nanoparticles formed within the polymer matrix, not the modulus of an individual CNC particle. The percolation volume fraction of the rigid phase, which is the volume fraction of CNC nanoparticles active in transferring stress, is obtained from the calculated geometrical percolation volume of CNC (ϕ_c) according to eqs 9 and 10:[1]

$$\psi = 0 \qquad \phi < \phi_c \tag{9}$$

$$\psi = \phi\left(\frac{\phi - \phi_c}{1 - \phi_c}\right)^{0.4} \qquad \phi \geq \phi_c \tag{10}$$

The modulus of the CNC network formation in polymer matrices and the CNC percolation volume fraction are two key parameters in eq 8. They are not easy to measure. A modulus value of 15 GPa for the CNC network has been suggested on the basis of DMA experiments for CNC films in the tensile mode.[1] It has also been suggested that eq 11 be used to estimate CNC percolation volume fraction:

$$\phi_c = \frac{0.7}{P} \tag{11}$$

where P is the CNC aspect ratio. The maximum value of P was 17 on the basis of AFM and TEM morphological analyses.[31] The red line in Figure 12a shows the model predictions of Young's modulus for PP nanocomposites versus CNC weight fraction according to eq 8 using the above-mentioned suggested values for ϕ_c and G_{np}. At low CNCSFD concentrations (1.5

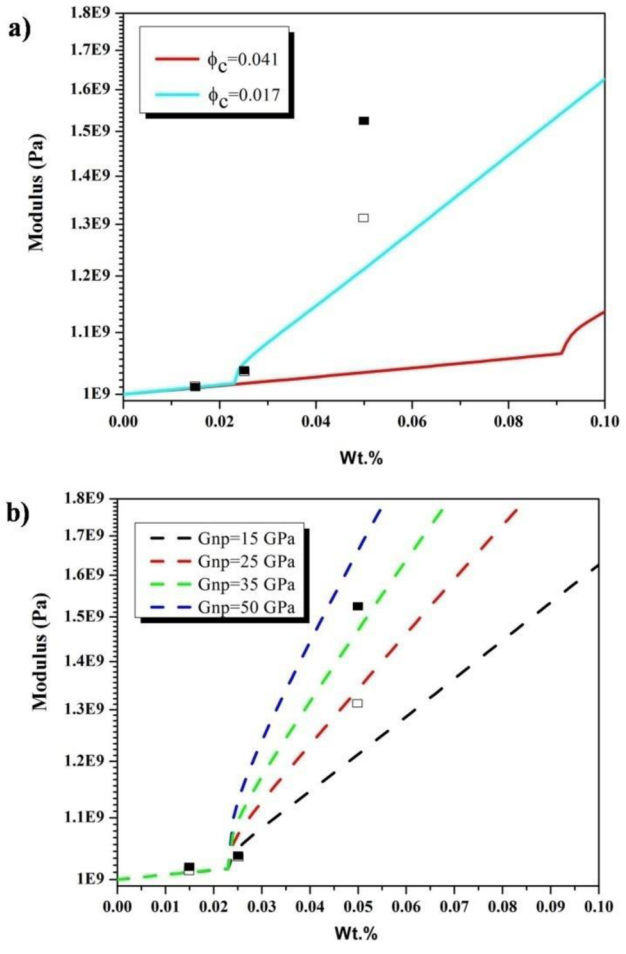

Figure 12. Comparison of experimental modulus data with values predicted by the percolation model (eq 8) at (a) two volume percolation fractions and (b) different strengths of the rigid phase.

and 2.5 wt %) with either the weblike structure (■) or the spherical foam structure (□), the experimental results were in the range of model predictions. It is noteworthy that eq 8 is designed for concentrations above the percolation threshold. Thus, it is more reasonable to verify the validity of this model at high CNC concentrations where a network is formed. The experimental modulus results for PPCNCSFD1-5 and PPCNCSFD2-5 were higher than the values predicted by eq 8. It is more reasonable to use the rheological percolation estimates to obtain an approximation of the geometrical percolation volume fraction (1.74 vol %). Figure 12a also shows the model prediction of Young's modulus of PP nanocomposites versus CNC weight fraction using 1.74 vol % as the percolation volume fraction of CNC (cyan line). Still, there is a difference between the experimental and model-predicted values at high CNC concentrations. There are some reasons for the disparities between the experimental values and model predictions. The percolation model has been used mainly in the rubbery region of amorphous polymers,[8,50−52] where the modulus of the polymer is 2 or 3 orders of magnitude lower than that of the CNC network. For a semicrystalline polymer (here PP), this may not be appropriate, and another micromechanical model should be used (discussed later). Moreover, for polymer melt systems containing an anisotropic filler, the determination of the exact volume fraction is difficult, as particles are usually in aggregated structures. Another reason stems from the estimated value of 15 GPa for the CNC network. The strength of the network depends on the state of dispersion and the CNC concentration, as discussed in Rheological Measurements. Contrary to the solution-based method, in melt mixing of polymer/CNC nanocomposites the network structure of CNC in the polymer melt could be different. The results of the model using rheological percolation at different modulus values of the CNCSFD network (i.e., 25, 35, and 50 GPa) are shown in Figure 12b. The results of the model and the experimental data were almost superimposed at values of 25 and 35 GPa for PP/CNCSFD2 and PP/CNCSFD1, respectively. The results are in good agreement with the rheological properties, where the yield stress for samples containing CNCSFD1 was higher than that for samples containing CNCSFD2. In other words, two different types of networks could be formed. Therefore, different modulus values should be assigned to the formed networks. It is not reasonable to use the modulus value based on CNC film measurements. As shown in Rheological Measurements, the rigidity of the resultant CNC network in the PP matrix depends on the structure of the CNCSFD particles. Moreover, polymer−filler interactions and the number of CNC nanoparticles participating in network formation should influence the strength of the network.

The Halpin−Kardos semiempirical model,[53] which is based on the mean-field approach, was proposed to estimate the modulus of randomly oriented nanocomposites, G_c, in terms of the parameters E_c and ν_{12} (see eq 24). These parameters are given by the following equations:

$$E_c = \frac{4U_2(U_1 - U_2)}{U_1} \tag{12}$$

in which

$$U_2 = \frac{(Q_{11} + Q_{22} - 2Q_{12} + 4Q_{66})}{8} \tag{13}$$

and

$$U_1 = \frac{(3Q_{11} + 3Q_{22} + 2Q_{12} + 4Q_{66})}{8} \tag{14}$$

where

$$Q_{11} = \frac{E_L}{(1 - \nu_{21}\nu_{12})} \tag{15}$$

$$Q_{22} = \frac{E_T}{(1 - \nu_{21}\nu_{12})} \tag{16}$$

$$Q_{12} = \nu_{12}Q_{22} \tag{17}$$

and Q_{66} is the shear modulus. Also,

$$\nu_{21} = \frac{E_T}{E_L} \tag{18}$$

$$\nu_{12} = \nu_p(1 - \phi) + \nu_{np}\phi \tag{19}$$

$$\eta_i = \frac{\frac{E_{npi}}{E_p} - 1}{\frac{E_{npi}}{E_p} + 1} \qquad i = T, L \tag{20}$$

and

$$E_i = \frac{(1 + \phi\zeta_i)}{(1 - \phi\zeta_i)} \qquad i = T, L \tag{21}$$

with

$$\zeta_L = 2P \tag{22}$$

and

$$\zeta_T = 2 \tag{23}$$

Finally, G_c is calculated as

$$G_c = \frac{E_c}{2(1 + \nu_{12})} \tag{24}$$

The details of the Halpin−Kardos model can be found elsewhere.[53,54] Values of 1 GP, 147 GP, 15 GP, 0.45, and 0.3 were used for the PP modulus (E_p), the longitudinal (E_{npL}) and transverse (E_{npT}) moduli of CNC, and the Poisson's ratios of the PP matrix (ν_p) and CNC (ν_{np}), respectively. Figure 13 displays the predicted values of the modulus at different CNC aspect ratios (P = 5, 10, 20, 30, and 40). There is good agreement between the theoretical and experimental data at low CNC concentration with an aspect ratio of 5. This aspect ratio is lower than the value for individual CNC particles (P = 11).[31] This disparity can be attributed to the CNC dispersion morphology in PP, which likely shows aggregated CNC nanoparticles rather than individuals. The model gives better results with aspect ratios of 30 and 20 for 5 wt % CNCSFD2 and CNCSFD1, respectively. One reason is that at high CNC concentrations, large-scale connectivity of CNC nanoparticles could have the effect of a high effective aspect ratio. In fact, the shape factor parameter of the Halpin−Kardos model (ζ) would be different at low and high CNC concentrations. Important assumptions of the Halpin−Kardos model include uniform morphology incorporating well-dispersed particles and perfect adhesion between the filler and matrix, which are not satisfied in most cases, thus leading to some estimation errors. Finally, unlike percolation models, the Halpin−Kardos model does not

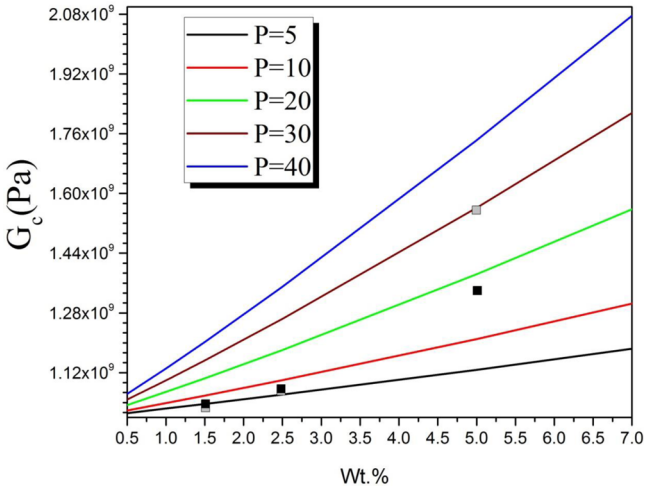

Figure 13. Comparison of experimental modulus values with predictions of the Halpin–Kardos model (eq 24).

account for filler–filler interactions, which occur at high filler concentrations.

CONCLUSION

PP/CNC nanocomposites incorporating CNC agglomerates prepared using different drying techniques (spray drying, freeze drying, and spray-freeze drying) were prepared via melt compounding. Both microscopy and rheology characterization techniques suggested that the CNC particles obtained using the novel spray-freeze drying technique yielded nanocomposites with significantly better dispersion in the PP matrix. Linear viscoelasticity tests are very sensitive to the filler dispersion in the polymer melt. The low-frequency rheological characteristics (loss modulus, storage modulus, and complex viscosity) increased significantly upon addition of CNCSFD. Below the rheological percolation threshold (ca. 2.5 wt % CNC), the high interfacial area resulting from the high level of dispersion in samples incorporating CNCSFD was credited for the significant rise in the magnitudes of the above rheological parameters. The presence of a 3D network determines the rheological properties beyond the percolation concentration of CNCSFD. SAOS and stress relaxation tests indicated that the polymer matrix was responsible for the short-time response (at high frequencies), while the 3D network structure was responsible for the long-time rheological responses (at low frequencies). Shear thinning behavior was observed upon incorporation of CNCSFD in PP melts at low shear rates. The magnitudes of the linear and nonlinear rheological properties of PP samples containing CNCSFD with a weblike structure were higher than those containing CNCSFD with a spherical foam structure. Dynamic mechanical analysis showed that at room temperature the Young's modulus for samples containing CNCSFD with a weblike structure was 60% higher than for neat PP.

ASSOCIATED CONTENT

Supporting Information

Strain sweep (Figure S.1), yield stress plot for curve fitting of eq 3 (Figure S.2), the effect of flow history (Figure S.3), stress relaxation (Figure S.4), and TGA and DTGA data for CNC (Figure S.5). This material is available free of charge via the Internet at http://pubs.acs.org.

AUTHOR INFORMATION

Corresponding Author

*E-mail: musa.kamal@mcgill.ca.

Notes

The authors declare no competing financial interest.

ACKNOWLEDGMENTS

The authors acknowledge financial support from the Natural Sciences and Engineering Research Council of Canada (NSERC), McGill University, CREPEQ, and the NIPMMP Strategic Network. FPInnovations donated the CNC used in this project. The authors thank Professor Paula Wood-Adams for use of the rheometry facility in her laboratory.

REFERENCES

(1) Favier, V.; Chanzy, H.; Cavaille, J. Y. Polymer Nanocomposites Reinforced by Cellulose Whiskers. *Macromolecules* **1995**, *28*, 6365–6367.

(2) Hajji, P.; Cavaille, J. Y.; Favier, V.; Gauthier, C.; Vigier, G. Tensile Behavior of Nanocomposites from Latex and Cellulose Whiskers. *Polym. Compos.* **1996**, *17*, 612–619.

(3) Araki, J.; Wada, M.; Kuga, S.; Okano, T. Flow Properties of Microcrystalline Cellulose Suspension Prepared by Acid Treatment of Native Cellulose. *Colloids Surf., A* **1998**, *142*, 75–82.

(4) Ranby, B. G. Aqueous Colloidal Solutions of Cellulose Micelles. *Acta Chem. Scand.* **1949**, *3*, 649–650.

(5) Paralikar, S. A.; Simonsen, J.; Lombardi, J. Poly(vinyl alcohol)/Cellulose Nanocrystal Barrier Membranes. *J. Membr. Sci.* **2008**, *32*, 248–258.

(6) Roohani, M.; Habibi, Y.; Belgacem, N.-M.; Ebrahim, G.; Karimi, A.-N.; Dufresne, A. Cellulose Whiskers Reinforced Polyvinyl Alcohol Copolymers Nanocomposites. *Eur. Polym. J.* **2008**, *44*, 2489–2498.

(7) Pranger, L.; Tannenbaum, R. Biobased Nanocomposites Prepared by in Situ Polymerization of Furfuryl Alcohol with Cellulose Whiskers or Montmorillonite Clay. *Macromolecules* **2008**, *41*, 8682–8687.

(8) Dufresne, A.; Cavaillé, J.-Y.; Helbert, W. Thermoplastic Nanocomposites Filled with Wheat Straw Cellulose Whiskers. Part II: Effect of Processing and Modeling. *Polym. Compos.* **1997**, *18*, 198–210.

(9) Samir, M. A. S.; Alloin, F.; Paillet, M.; Dufresne, A. Preparation of Cellulose Whiskers Reinforced Nanocomposites from an Organic Medium Suspension. *Macromolecules* **2004**, *37*, 4313–4316.

(10) Neus Angles, M.; Dufresne, A. Plasticized Starch/Tunicin Whiskers Nanocomposites. 1. Structural Analysis. *Macromolecules* **2000**, *33*, 8344–8353.

(11) Samir, M. A. S.; Alloin, F.; Sanchez, J. Y.; Dufresne, A. Cellulose Nanocrystals Reinforced Poly(Oxyethylene). *Polymer* **2004**, *45*, 4149–4157.

(12) Gopalan Nair, K.; Dufresne, A. Crab Shell Chitin Whisker Reinforced Natural Rubber Nanocomposites. 1. Processing and Swelling Behavior. *Biomacromolecules* **2003**, *4*, 657–665.

(13) Gopalan Nair, K.; Dufresne, A. Crab Shell Chitin Whisker Reinforced Natural Rubber Nanocomposites. 2. Mechanical Behavior. *Biomacromolecules* **2003**, *4*, 666–674.

(14) Gopalan Nair, K.; Dufresne, A.; Gandini, A.; Belgacem, M. N. Crab Shell Chitin Whiskers Reinforced Natural Rubber Nanocomposites. 3. Effect of Chemical Modification of Chitin Whiskers. *Biomacromolecules* **2003**, *4*, 1835–1842.

(15) Heux, L.; Ljungberg, N.; Cavaille, J. Y. Nanocomposites of Isotactic Polypropylene Reinforced with Rod-Like Cellulose Whiskers. *Polymer* **2006**, *47*, 6285–6292.

(16) Ljungberg, N.; Bonini, C.; Bortolussi, F.; Boisson, C.; Heux, L.; Cavaillé, J. Y. New Nanocomposite Materials Reinforced with Cellulose Whiskers in Atactic Polypropylene: Effect of Surface and Dispersion Characteristics. *Biomacromolecules* **2005**, *6*, 2732–2739.

(17) Junior de Menezes, A.; Siqueira, G.; Curvelo, G. A. S.; Dufresne, A. Extrusion and Characterization of Functionalized Cellulose Whiskers Reinforced Polyethylene Nanocomposites. *Polymer* **2009**, *50*, 4552−4563.
(18) Chazeau, L.; Cavaillé, J. Y.; Canova, G.; Dendievel, R.; Boutherin, B. Viscoelastic Properties of Plasticized PVC Reinforced with Cellulose Whiskers. *J. Appl. Polym. Sci.* **1999**, *71*, 1797−1808.
(19) Garcia de Rodriguez, N.-L.; Thielemans, W.; Dufresne, A. Sisal Cellulose Whiskers Reinforced Polyvinyl Acetate Nanocomposites. *Cellulose* **2006**, *13*, 261−270.
(20) Siaueira, G.; Bras, J.; Dufresne, A. Cellulose Whiskers versus Microfibrils: Influence of the Nature of the Nanoparticle and Its Surface Functionalization on the Thermal and Mechanical Properties of Nanocomposites. *Biomacromolecules* **2009**, *10*, 425−432.
(21) Oksman, K.; Mathew, A. P.; Bondeson, D.; Kvien, I. Manufacturing Process of Cellulose Whiskers/Polylactic Acid Nanocomposites. *Compos. Sci. Technol.* **2006**, *66*, 2776−2784.
(22) Bondeson, D.; Oksman, K. Polylactic Acid/Cellulose Whisker Nanocomposites Modified by Polyvinyl Alcohol. *Composites, Part A* **2007**, *38*, 2486−2492.
(23) Yu, J.; Ai, F.; Dufresne, A.; Gao, S.; Huang, J.; Chang, P.-R. Structure and Mechanical Properties of Poly(lactic acid) Filled with (Starch Nanocrystal)-*graft*-Poly(ε-caprolactone). *Macromol. Mater. Eng.* **2008**, *293*, 763−770.
(24) Lin, N.; Chen, G.; Huang, J.; Dufresne, A.; Chang, P. R. Effects of Polymer-Grafted Natural Nanocrystals on the Structure and Mechanical Properties of Poly(Lactic Acid): A Case of Cellulose Whisker-*graft*-Polycaprolactone. *J. Appl. Polym. Sci.* **2009**, *113*, 3417−3425.
(25) Sanchez-Garcia, M.; Lagaron, J. On the Use of Plant Cellulose Nanowhiskers To Enhance the Barrier Properties of Polylactic Acid. *Cellulose* **2010**, *17*, 987−1004.
(26) Ruiz, M. M.; Cavaillé, J.-Y.; Dufresne, A.; Gerard, J. F.; Graillat, C. Processing and Characterization of New Thermoset Nanocomposites Based on Cellulose Whiskers. *Compos. Interfaces* **2000**, *7*, 117−131.
(27) Abdelmouleh, M.; Boufi, S.; Belgacem, M. N.; Dufresne, A.; Gandini, A. Modification of Cellulose Fibers with Functionalized Silanes: Effect of the Fiber Treatment on the Mechanical Performances of Cellulose−Thermoset Composites. *J. Appl. Polym. Sci.* **2005**, *98*, 974−984.
(28) Jiang, L.; Morelius, E.; Zhang, J.; Wolcott, M.; Holbery, J. Study of the Poly(3-hydroxybutyrate-*co*-3-hydroxyvalerate)/Cellulose Nanowhisker Composites Prepared by Solution Casting and Melt Processing. *J. Compos. Mater.* **2008**, *42*, 2629−2645.
(29) Bondeson, D.; Oksman, K. Dispersion and Characteristics of Surfactant Modified Cellulose Whiskers Nanocomposites. *Compos. Interfaces* **2007**, *14*, 617−630.
(30) Beck, S.; Bouchard, J.; Berry, R. Dispersibility in Water of Dried Nanocrystalline Cellulose. *Biomacromolecules* **2012**, *13*, 1486−1494.
(31) Khoshkava, V.; Kamal, M. R. Effect of Surface Energy on Dispersion and Mechanical Properties of Polymer/Nanocrystalline Cellulose Nanocomposites. *Biomacromolecules* **2013**, *14*, 3155−3163.
(32) Utracki, L. A. Flow and Flow Orientation of Composites Containing Anisometric Particles. *Polym. Compos.* **1986**, *7*, 274−282.
(33) Shenoy, A. V. *Rheology of Filled Polymer Systems*; Springer: Dordrecht, The Netherlands, 1999; Chapter 6, p 246.
(34) Aranguren, M. I.; Mora, E.; Degroot, J. V.; Macosko, C. W. Polypropylene/Montmorillonite Nanocomposites. Review of the Synthetic Routes and Materials Properties. *J. Rheol.* **1992**, *36*, 1165−1182.
(35) Shih, W. H.; Shih, W. Y.; Kim, S. I.; Aksay, A. I. Scaling Behavior of the Elastic Properties of Colloidal Gels. *Phys. Rev. A* **1990**, *42*, 4772−4779.
(36) Ren, J.; Silva, A. S.; Krishnamoorti, R. Linear Viscoelasticity of Disordered Polystyrene−Polyisoprene Block Copolymer Based Layered-Silicate Nanocomposites. *Macromolecules* **2000**, *33*, 3739−3746.
(37) Isichenko, M. B. Percolation, Statistical Topography and Transport in Random Media. *Rev. Mod. Phys.* **1992**, *64*, 961−1043.
(38) Larson, R. G. *The Structure and Rheology of Complex Fluids*; Oxford University Press: New York ,1998; Chapter 1, p 15.
(39) Batthacharya, S. N.; Gupta, R. K.; Kamal, M. R. In *Polymeric Nanocomposites: Theory and Practice*; Hanser: Munich, 2008; Chapter 4, pp 145−169.
(40) Litchfield, D. W.; Baird, D. G. The Rheology of High Aspect Ratio Nanoparticle Filled Liquid. *Rheol. Rev.* **2006**, 1−60.
(41) Krishnamoorti, R.; Giannelis, E. P. Rheology of End-Tethered Polymer Layered Silicate Nanocomposites. *Macromolecules* **1997**, *30*, 4097−4102.
(42) Galgali, G.; Ramesh, C.; Lele, A. A Rheological Study on the Kinetics of Hybrid Formation in Polypropylene Nanocomposites. *Macromolecules* **2001**, *34*, 852−858.
(43) Solomon, M. J.; Almusallam, A.-S.; Seefeldt, K. F.; Somwangthanaroj, A.; Varadan, P. Rheology of Polypropylene/Clay Hybrid Materials. *Macromolecules* **2001**, *34*, 1864−1872.
(44) Jouault, N.; Vallat, P.; Dalmas, F.; Said, S.; Jestin, J.; Boué, F. Cellulose Poly(ethylene-*co*-vinyl acetate) Nanocomposites Studied by Molecular Modeling and Mechanical Spectroscopy. *Macromolecules* **2009**, *42*, 2031−2040.
(45) Song, Y.; Zheng, Q. Linear Viscoelasticity of Polymer Melts Filled with Nano-Sized Fillers. *Polymer* **2010**, *51*, 3262−3268.
(46) Abbasi, S.; Carreau, P. J.; Derdouri, A. Flow Induced Orientation of Multiwalled Carbon Nanotubes in Polycarbonate Nanocomposites: Rheology, Conductivity and Mechanical Properties. *Polymer* **2010**, *51*, 922−935.
(47) Ren, J.; Krishnamoorti, R. Nonlinear Viscoelastic Properties of Layered-Silicate-Based Intercalated Nanocomposites. *Macromolecules* **2003**, *36*, 4443−4451.
(48) Favier, V.; Cavaille, J. Y.; Canova, G. R.; Shrivastava, S. C. Mechanical Percolation in Cellulose Whisker Nanocomposites. *Polym. Eng. Sci.* **1997**, *37*, 1732−1739.
(49) Takayabagi, M.; Uemura, S.; Minami, S. Application of Equivalent Model Method to Dynamic Rheo-Optical Properties of Crystalline Polymer. *J. Polym. Sci., Polym. Symp.* **1964**, *5*, 113−122.
(50) Favier, V.; Canova, G.-R.; Cavaillé, J.-Y.; Chanzy, H.; Dufresne, A.; Gauthier, C. Nanocomposite Materials from Latex and Cellulose Whiskers. *Polym. Adv. Technol.* **1995**, *6*, 351−355.
(51) Dubief, D.; Samain, E.; Dufresne, A. Polysaccharide Microcrystals Reinforced Amorphous Poly(β-hydroxyoctanoate) Nanocomposite Materials. *Macromolecules* **1999**, *32*, 5765−5771.
(52) Dufresne, A.; Kellerhals, M.-B.; Witholt, B. Transcrystallization in Mcl-PHAs/Cellulose Whiskers Composites. *Macromolecules* **1999**, *32*, 7396−7401.
(53) Halpin, J. C.; Kardos, J.-L. The Halpin−Tsai Equations: A Review. *Polym. Eng. Sci.* **1976**, *16*, 344−352.
(54) Halpin, J. C. *Effects of Environmental Factors on Composite Materials*; Technical Report AFML-TR-67-423; Air Force Materials Laboratory: Wright-Patterson Air Force Base, OH, 1969.